

HOSTED BY



Contents lists available at ScienceDirect

Journal of King Saud University – Science

journal homepage: [www.sciencedirect.com](http://www.sciencedirect.com)

Original article

# A green approach for the degradation of toxic textile dyes by nickel oxide (NiO-SD) NPs: Photocatalytic and kinetic approach



J.P. Shubha<sup>a,\*</sup>, H.S. Savitha<sup>b</sup>, R.C. Patil<sup>c</sup>, Mohamed E. Assal<sup>d</sup>, Mohammed Rafi Shaik<sup>d</sup>, Mufisir Kuniyil<sup>d</sup>, Osamah Alduhaish<sup>d</sup>, Narsimhaswamy Dubasi<sup>e</sup>, Syed Farooq Adil<sup>d,\*</sup>

<sup>a</sup> Department of Chemistry, Sri Jayachamarajendra College of Engineering, JSS S&T University, Mysuru 570006, India

<sup>b</sup> Department of Chemistry, SJB INSTITUTE OF TECHNOLOGY, Dr. Vishnuvardhan Road, Bengaluru-560060, India

<sup>c</sup> Department of Electronics and Communication Engineering, Jain College of Engineering Belagavi - 590006, Karnataka, India

<sup>d</sup> Department of Chemistry, College of Science, King Saud University, P.O. Box 2455, Riyadh 11451, Saudi Arabia

<sup>e</sup> 12001 Belcher Rd S, Apt N226, Largo, FL 33773-5039, USA

## ARTICLE INFO

### Article history:

Received 16 February 2023

Revised 20 May 2023

Accepted 22 June 2023

Available online 11 July 2023

### Keywords:

Green synthesis  
NiO-NPs  
Methylene blue  
Malachite Green  
Photocatalysis  
Degradation

## ABSTRACT

By utilizing the combustion process, nanoparticles can be produced quickly, easily, and in an environmentally friendly manner. In this study, sheep dung is employed as fuel for the synthesis of nickel oxide nanoparticles (NiO-SD), and characterization techniques such as XRD, FTIR, UV, FESEM, and EDX, are used to confirm the as-desired nanoparticles. Malachite green (MG) and methylene blue (MB), respectively, are used as benchmark dyes to measure the photocatalytic effectiveness of the material and systematically investigated the effects of the light source, dye concentration, dose of photocatalyst, and pH value on the effectiveness of photocatalyst and photodegradation kinetics. It is found that the NiO-SD, when exposed to UV light, shows good removal effectiveness of the MB and MG dyes, according to the photodegradation data of 99.9% and 96.8%, respectively. The remarkable photodegradation efficiency of MB and MG dyes over the developed photocatalyst is also explained by a plausible photo-catalytic process. The green-manufactured photocatalyst can be a promising for ecological applications such as wastewater remediation.

© 2023 The Author(s). Published by Elsevier B.V. on behalf of King Saud University. This is an open access article under the CC BY license (<http://creativecommons.org/licenses/by/4.0/>).

## 1. Introduction

In the current era human and aquatic lives are greatly affected by highly stable toxic dyes and their effluents which are generated by many industries like textile dyeing, plastic dyeing, paper, pesticides, fertilizers, leather dyeing, food processing, petrochemical industries (Zollinger 2003, Fosso-Kankeu et al. 2020, Tsai et al. 2023). These industries discharge effluents containing toxic dyes which are difficult to degrade due to their chemical structure which made those dyes highly stable. These poisonous organic

dyes cause intense environmental pollution. These damaging dyes are degraded by many techniques such as chemical oxidation, adsorption, precipitation, ion exchange, biological, reverse osmosis, and photocatalysis (Zollinger 2003). Due to inefficient and expensive procedures, these methods are likely to discharge dangerous pollutants into the water bodies. Hence cost-effective and environmentally benign substitute procedures are essential to decrease the above-mentioned complications for the decomposition of dyes present in effluents. Among the approaches recommended so far, Advanced-Oxidation-Process (AOP), is known to be one of the best techniques for the decomposition of toxic dyes in effluent water using semiconductor-based photocatalysts (Pouretedal et al. 2009, Alharthi et al. 2020, Dalal et al. 2023), mostly nanoparticles in nature, are widely used because of their high efficiency, and eco-friendly nature (Mills et al. 1993, Lavand and Malghe 2015, Hassaan et al. 2017, Navarro et al. 2017, Natarajan et al. 2018, Natarajan et al. 2018, Pirhashemi et al. 2018, Belver et al. 2019, Di et al. 2019). Several nanoparticles such as Fe, Sn, and Zn as well as the bimetallic combination has

\* Corresponding authors.

E-mail addresses: [shubhapranesh@gmail.com](mailto:shubhapranesh@gmail.com) (J.P. Shubha), [sfadi@ksu.edu.sa](mailto:sfadi@ksu.edu.sa) (S. Farooq Adil).

Peer review under responsibility of King Saud University.



Production and hosting by Elsevier

<https://doi.org/10.1016/j.jksus.2023.102784>

1018-3647/© 2023 The Author(s). Published by Elsevier B.V. on behalf of King Saud University. This is an open access article under the CC BY license (<http://creativecommons.org/licenses/by/4.0/>).

provided better degradation rates (Tammina et al. 2018, Mirgane et al. 2021, Mahlaule-Glory et al. 2022, Padre et al. 2022, Gan et al. 2023). Among these, NiO-NPs has been extensively studied and have also been employed for the degradation of dye and other pollutants (Jayakumar et al. 2017, Khairnar and Shrivastava 2019, Akbari et al. 2020, Barzinjy et al. 2020, Ramesh 2021, Qamar et al. 2022) along with various other uses such as catalysts, battery cathodes, gas sensors, magnetic materials, antimicrobial (Singh et al. 2018) etc. Due to its strong magnetic and electrical properties, NiO, a p-type semiconductor (Al Boukhari et al. 2020), is a subject of extensive research. Due to the immense importance of these nanoparticles, there are extensive efforts for the development of various methodologies for their synthesis of these amazing nanoparticles, including green protocols. A variety of green methods for the preparation of metal oxide nanoparticles have been reported such as plant-based synthesis, microbial synthesis, etc. One more method that has attracted attention is solution combustion synthesis, which can be included in the list of green methodologies of many researchers in the modern period (Mills et al. 1993, Capek 2006, Lavand and Malghe 2015, Hassaan et al. 2017, Navarro et al. 2017, Pirhashemi et al. 2018, Singh et al. 2018, Belver et al. 2019, Di et al. 2019).

In this work, an attempt is made to synthesize NiO NPs as photocatalysts in ecologically friendly and inexpensive combustion methodology using the sheep dung as fuel [NiO NPs synthesized using sheep dung as fuel are designated as NiO-SD NPs] to achieve high photo-decomposition activity over two organic chronic dyes (MB and MG dyes) as demonstrated in Scheme 1. The prepared NiO-SD NPs are employed as photocatalyst for the removal of dyes in an aqueous solution in presence of various light sources. Additionally, the effect of several catalytic factors such as irradiation time, dye concentration (ppm), photocatalyst amount, and pH value on the photocatalytic decomposition of MB and MG dyes are also investigated. The photocatalytic data disclosed that the NiO-SD NPs photocatalyst exhibited superior photocatalytic efficiency for the degradation of MB and MG dyes under UV irradiation, and a 97.7% and 96.8% of MB and MG dyes are decomposed within 100 min, respectively, under the optimal conditions.

## 2. Materials and methods

### 2.1. Materials

Analytical grade nickel acetate tetrahydrate,  $\text{Ni}(\text{OCOCH}_3)_2 \cdot 4\text{H}_2\text{O}$  (Merck) is utilized without further purification. Sheep dung is collected and dried under sunlight for 12 days and used as fuel.

### 2.2. Synthesis of NiO-SD NPs photocatalyst

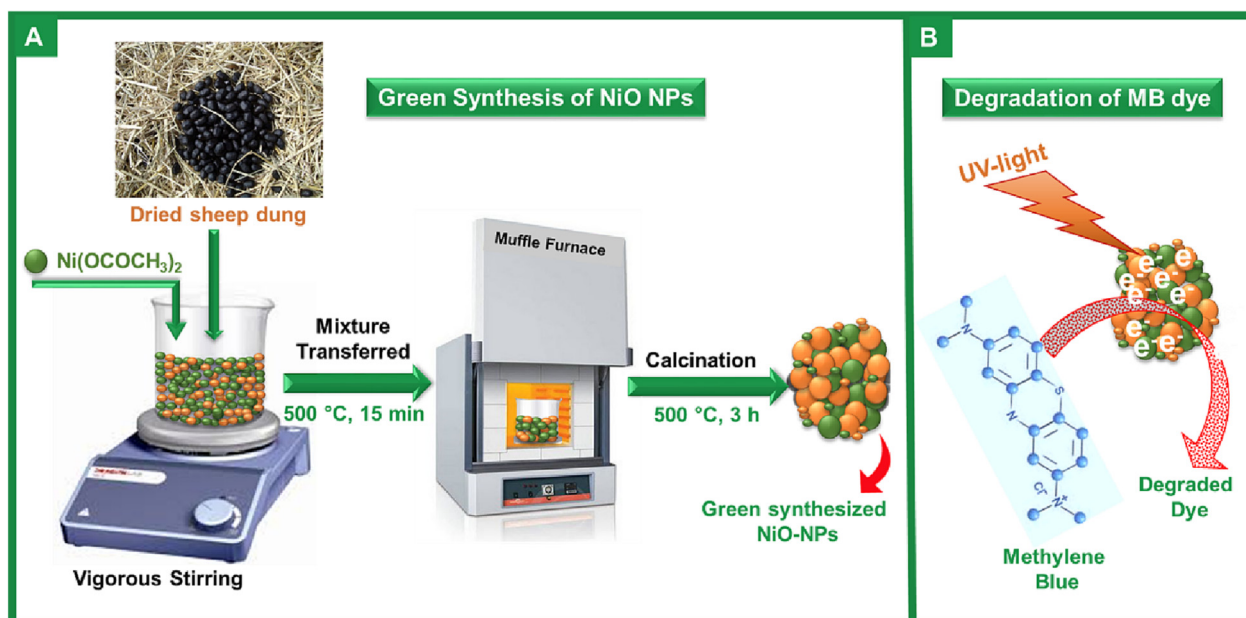
The synthesis was carried out by using nickel acetate tetrahydrate ( $\text{Ni}(\text{OCOCH}_3)_2 \cdot 4\text{H}_2\text{O}$ , 98%, Sigma Aldrich) and dried sheep dung. The dried sheep dung was mixed with aqueous solution of  $\text{Ni}(\text{OCOCH}_3)_2 \cdot 4\text{H}_2\text{O}$  by constant stirring. The stirred solution was kept in a preheated muffle furnace for 15 min at  $500 \pm 10$  °C followed by calcination at 500 °C for 3 h. The obtained black-coloured product was stored in airtight vials.

## 3. Results and discussion

### 3.1. XRD analysis

The as-prepared NiO-SD NPs are subjected to X-ray diffraction analysis and the obtained diffraction pattern is shown in Fig. 1a. The diffraction pattern obtained reveals the crystallinity and purity of the NiO-SD NPs. The diffraction pattern matches with the standard JCPDS card no. 4–835, which shows that the NiO-SD NPs obtained is cubic in structure with lattice constants  $a = b = c = 4.1769$  Å, which belongs to the space group: Fm-3 m. The peaks at  $37^\circ$ ,  $43^\circ$ , and  $63^\circ$  were assigned to (111), (200), (220) and (311) planes, respectively (Salavati-Niasari et al. 2010, Patil et al. 2018). The average crystallite sizes were determined ( $2\theta = 37, 43, 63$ ) and found to be 8.79, 8.92 and 8.04 nm, respectively using Debye Scherer's formula (Eq. (1))

$$\text{Crystalline size}(D), D = (k\lambda/\beta \cos \theta) \quad (1)$$



**Scheme 1.** Schematic representation of as synthesized NiO-SD NPs and their photocatalytic activity towards dye degradation.

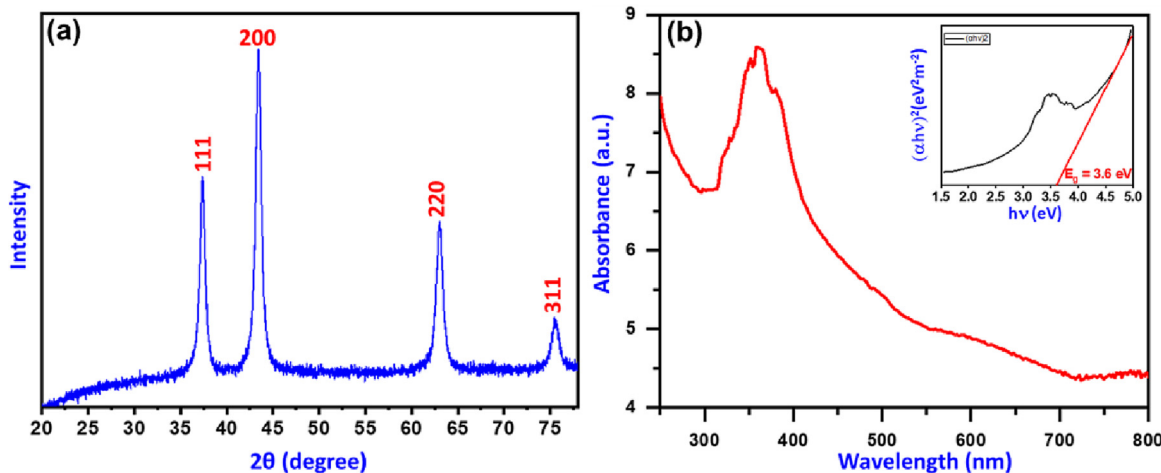


Fig. 1. (a) XRD pattern and (b) UV-vis and band gap spectra (inset) of as synthesized NiO-SD NPs.

### 3.2. UV-vis analysis

Fig. 1b displays the UV-visible absorption spectra of as-fabricated NiO-SD NPs together with an inset Tauc plot. The absorbance maximum was noticed around 361 nm, which pointed to the formation of NiO-NPs. This is due to fundamental band-gap absorption, which is brought on by the electrical transition between the valence and conduction bands of Ni atoms, as has already been noticed. The direct band gap energy of NiO-SD NPs as they have been produced is anticipated to be 3.6 eV by extrapolating the straight line in the Tauc plot.

### 3.3. FTIR analysis

Fig. 2a depicts an analysis of NiO-SD NPs that were formed using FTIR spectroscopy. The spectral data demonstrate the formation of NiO-SD NPs with an intense peak related to the (Ni-O) stretching vibrations below the wavenumber of 500 cm<sup>-1</sup>, as has been previously reported in the literature (Sabouri et al. 2018). Other absorption peaks, such the broad peak at 1030 cm<sup>-1</sup>, are caused by absorbed CO<sub>2</sub>, which is most likely from the by-products of the burning of sheep dung during the synthesis of NiO-SD NPs.

### 3.4. Raman analysis

The as-prepared nanocrystalline NiO-SD NPs subjected to Raman spectroscopy, which reveals a spectrum of phonon-related and magnon-related Raman bands, a wide one-phonon (1P) band between ~300-600 cm<sup>-1</sup> and two-phonon (2P) bands at ~808 cm<sup>-1</sup>, ~966 cm<sup>-1</sup> and ~1052 cm<sup>-1</sup> along with a strong band around 514 cm<sup>-1</sup>. The strong band at 514 cm<sup>-1</sup> is characteristic of NiO-SD NPs (Gouadec and Colomban 2007). Additionally, the presences of low intensity two-magnon band at ~1551 cm<sup>-1</sup> corroborates the formation of nanoparticles as desired, which is usually a high-intensity band for bulk material (Fig. 2b) (Mironova-Ulmane et al. 2019). The results are in good agreement of the crystallite size calculated using the Debye Scherer equation.

### 3.5. SEM and EDX analysis

The topological characteristics of the as-obtained NiO-SD NPs are assessed using FE-SEM. The NiO-SD NPs images clearly display porosity on their surface while possessing irregular morphology (Fig. 3a). Additionally, the elemental composition is confirmed using EDX spectroscopy which is displayed in Fig. 3b. It demonstrates that the generated Nanoparticles contain the desired ele-

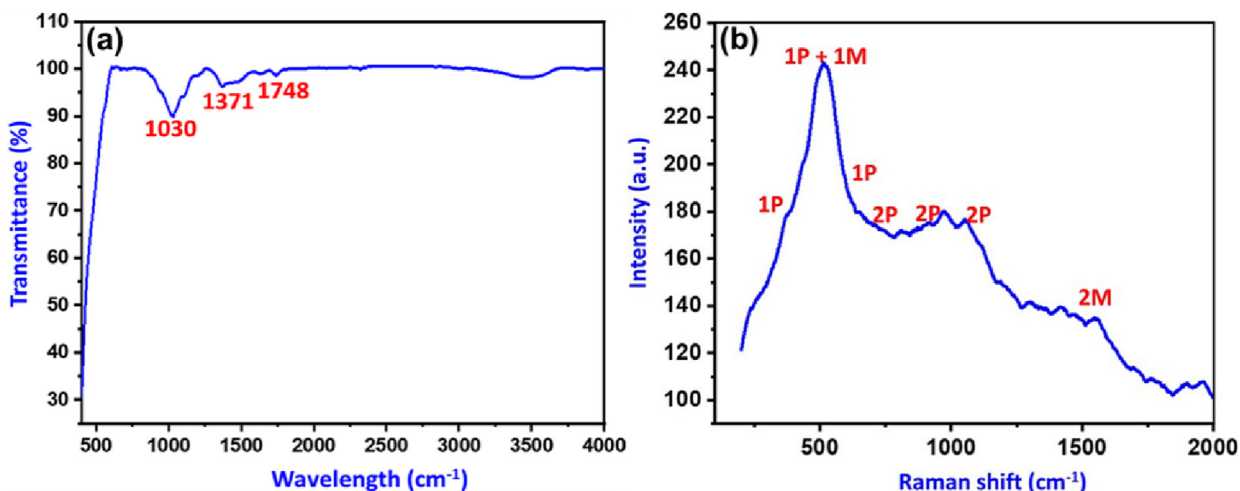


Fig. 2. (a) FTIR and (b) Raman spectrum of the as synthesized NiO-SD NPs.

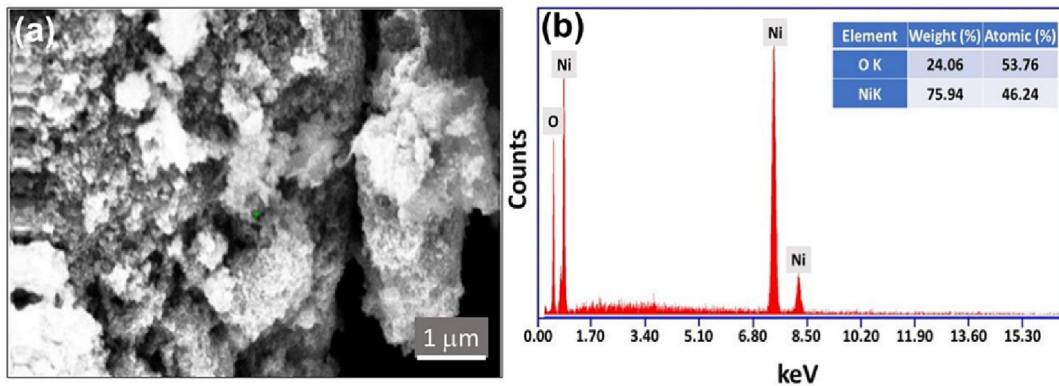


Fig. 3. (a) FE-SEM micrographs of the fabricated NiO-SD NPs and (b) EDX spectra of the prepared NiO-SD NPs.

mental composition, namely Ni and O, the atomic percentages obtained are displayed as inset (Fig. 3b).

### 3.6. Photo-degradation efficacy results

The fundamental objective of the present study is to employ the environment-friendly NiO-SD NPs as photo-catalyst for the photo-elimination of the hazardous MB and MG, harmful pollutants existing in the wastewater emissions from textile manufacturing. The photo-catalytic removal efficiency of the as-obtained NiO-SD NPs has been examined by varying the several catalytic parameters. According to theoretical studies, various factors determine the photocatalytic efficacy of the catalyst including, the crystal structure, band-gap, surface area, particle size, morphology, and quantities of free radical ions ( $\text{OH}^\bullet$ ) on the surface of the catalyst (Zhang et al. 2018). The proposed model described the generation of photo-produced charge carriers on surface of photo-catalyst by absorbing light and the generated electrons and holes will participate in the process or they do reunion. If the additional surface has provided for the electrons and holes, they will relocate where the electrons have trapped by catalyst, while the holes have caught by hydroxyl radicals to produce  $\text{OH}^\bullet$  and  $\text{HO}_2^\bullet$ . In case of metallic oxide nanoparticles, extra surface was available for relocation of electrons and holes and consequently the produced  $\text{OH}^\bullet$  were utilized efficaciously to dye photo-elimination process (Kumar et al. 2021). The data obtained from the UV-vis spectra, it was obvious that the prepared material is active in UV domain. Moreover, the band-gap calculated to be  $E_g = 3.6$  eV (Asgharian et al. 2019). This study meticulously assesses the photocatalytic parameters of lighting source, concentration of dye, catalyst dosage, and pH value, with MB and MG dyes have been chosen as the reference harmful dyes for photocatalytic elimination. The variation in absorption intensity between the peaks recorded at 663 nm (MB  $\lambda_{\text{max}}$ ) and 556 nm (MG  $\lambda_{\text{max}}$ ) is measured to aggregate the collected results. The initial dye concentration ( $C_i$ ) and final dye concentration ( $C_f$ ) in the photocatalytic protocol were calculated from the UV-vis spectrum and the degradation efficiency calculation for the MB and MG has conducted using the subsequent formula (2)

$$\text{Degradation activity (\%)} = \frac{C_i - C_f}{C_i} \times 100 \quad (2)$$

#### 3.6.1. Impact of source of light on MB and MG dyes photo-decomposition

The initial studies focus on the light source with the maximal degradation performance for the generated NiO-SD NPs. To get the best lighting source exhibits maximum photo-degradation of MB and MG dyes, three different lighting conditions including,

dark, visible light, and UV-irradiation were utilized in the experiments. The photo-catalytic data obtained was illustrated in Fig. 4. When the photo-elimination test was performed in dark condition, the photo-degradation of MB and MG dyes are disintegrating insignificantly and could be neglected. It has been noticed that only 3.0% of MB and 5.0% of MG dyes were degraded by NiO-SD NPs under dark conditions. Additionally, the degradation data from the tests conducted using visible light and UV-irradiation is compared, the attained results disclose that the removal of MB and MG under UV-irradiation is significantly higher than degradation attained using visible light. For UV-irradiation, the synthesized NiO-SD NPs efficaciously degrades 97.7% of MB dye substantially higher than visible light, which yielded just 19% decomposition at the identical time (100 min) as demonstrated in Fig. 4a. Similar to this, MG dye exhibited extremely higher degradation activity of 96.8% using UV-irradiation compared to visible light, which decomposed just 18.0% of MG at the similar circumstances (Fig. 4b). The UV-Vis spectrum (Fig. 1b) of NiO-SD NPs in good agreement with the data attained for the photo-elimination of MB and MG using UV-irradiation. According to afore mentioned observations, the decomposition efficacy of MB and MG in presence of UV-irradiation is higher than visible light. Thus, it can be concluded that the NiO-SD NPs are efficacious photocatalysts under UV-irradiation and remaining optimization experiments are performed in presence of UV-irradiation.

#### 3.6.2. Impact of photocatalyst amount on MB and MG dyes photo-decomposition

The appropriate photocatalyst dose is the important factor that influences the removal activity. Therefore, the catalyst concentration for the removal efficacy of MB and MG was investigated by varying dosage of NiO-SD NPs from 5 to 20 mg using UV-irradiation, whereas other parameters i.e., lighting source, dye concentration, and pH was kept constant. Obviously, the outcomes apparently illustrated that the MB and MG removal effectiveness is significantly affected by the photocatalyst dosage utilized (Fig. 5). The results revealed that, only 69.0% and 78.8% of MB and MG dye degradation are obtained, respectively, when a 5 mg of catalyst has employed. As anticipated, as the quantity of catalyst increased to 10 and 15 mg, an 88.0% and 97.7% degradation of MB and degradation of MG of 90.2% and 96.8% has attained, respectively. Notably, by increasing catalyst concentration to 20 mg led to a reduction in degradation performance and 82% for degradation of MB (Fig. 5a) and 92.0% for degradation of MG (Fig. 5b). The improvement in the decomposition efficacy was typically owing to the introducing additional active sites in the reaction that can produce more free radicals. When the amount of catalyst surpassed a critical border there will not be enough distance for the nanopar-

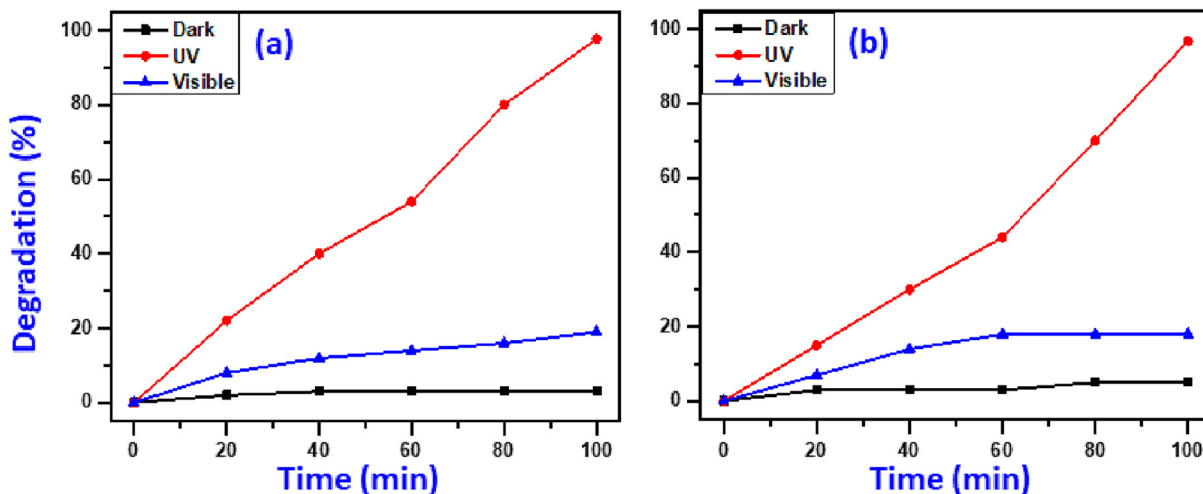


Fig. 4. Impact of lighting source on elimination of MB (a) and MG(b). (Circumstances: 15 mg catalyst dosage, 4 ppm dye conc., and 7pH value).

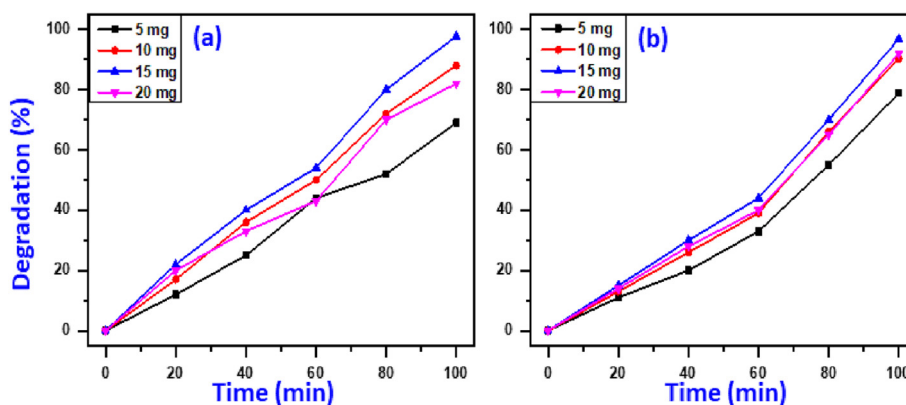


Fig. 5. Impact of catalyst dose on photo-elimination of MB (a) and MG (b). (Circumstances: 4 ppm dye conc., 7pH value, and UV-irradiation).

ticles to disperse in the medium and the nanoparticles will adhere to each other and agglomerated, could be due to the surface energy of particles. Consequently, the majority of the active sites were blocked and the photo degradation performance declined (Nguyen et al. 2018). As demonstrated in Fig. 5a and 5b), both MB and MG dyes exhibit the best photodecomposition efficacy at 15 mg photocatalyst dosage. Henceforth 15 mg is a suitable photocatalyst dosage for the maximal photo-catalytic removal of MB and MG.

### 3.6.3. Impact of MB and MG dyes concentration on removal activity

Influence of dye concentrations on photodecomposition efficacy of MB and MG was evaluated by varying dye concentration from 4 to 16 ppm employing UV-irradiation while the 15 mg catalyst dose and pH value of 7 keeping constant as illustrated in Fig. 6. The degradation data clearly displayed that the photo-degradation rate was inversely proportionate to MB and MG dyes concentration at same circumstances, which highest elimination efficiency has been observed at minimum concentration (4 ppm).The elimination activity of MB progressively dropped from 99.7% to 71.5% as MB concentration increased from 4 to 16 ppm (Fig. 6a).Similar trend occurs for photodegradation of MG dye, as MG concentration increases from 4 to 16 ppm, the photodecomposition efficacy of MG reduced from 99.9% to 80.0% (Fig. 6b). This abatement mainly attributed to the reduced light absorption on the surface of catalyst by increasing concentration of dye, which leads to decrease in the generation of OH\* ions which play a fundamental role in photo-

elimination process (Nguyen et al. 2018).As a consequence, the maximum removal effectiveness was attained at the MB and MG concentration of 4 ppm, so, 4 ppm concentration of dye has been chosen for further optimization tests.

### 3.6.4. Influence of pH on photodecomposition efficacy

The pH value usually has an explicit effect on photo-catalytic degradation of harmful dyes and the decomposition performance usually related to the amounts of hydroxyl radicals (OH\*) present in the medium, which increases the photo-degradation effectiveness several folds in high pH solutions. Fig. 7a and 7b display that the impact of pH on photocatalytic removal of MB and MG catalysed by NiO-SD NPs. The influence of pH of solution on photodecomposition of MB and MG has assessed at three pH values of 4, 7 and 10 with preserving other variables unaltered (4 ppm dye conc., 15 mg catalyst dosage and UV-irradiation).As it has predicted, the lowest decomposition performance was attained at minimum pH value (pH = 4) with 50.0% and 46.0% of MB and MG decomposed after 100 min, respectively. However, by increasing the pH, the NiO-SD NPs exhibited higher removal efficacy which degraded 80.0%, and 100% of MB dye within only 80 min at pH7, and 10, respectively (Fig. 7a). In addition, 96.8% and 100% of MG dye has been degraded within 100 min at pH7, and 10, respectively, at same photocatalytic circumstances (Fig. 7b).The observations distinctly demonstrated that the dye decomposition in basic solution is extremely higher than acidic solution, presumably scribed to higher pH values leads to production of negative charges

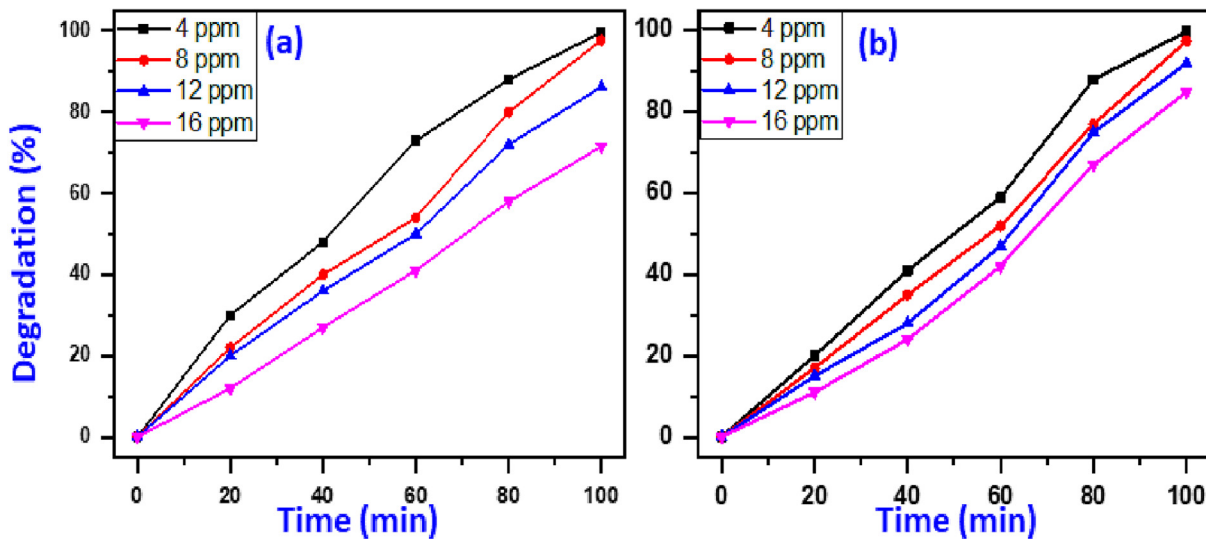


Fig. 6. Impact of dye concentration on elimination of MB(a) and MG(b). (Circumstances: 15 mg catalyst dosage, 7pH value, and UV-irradiation).

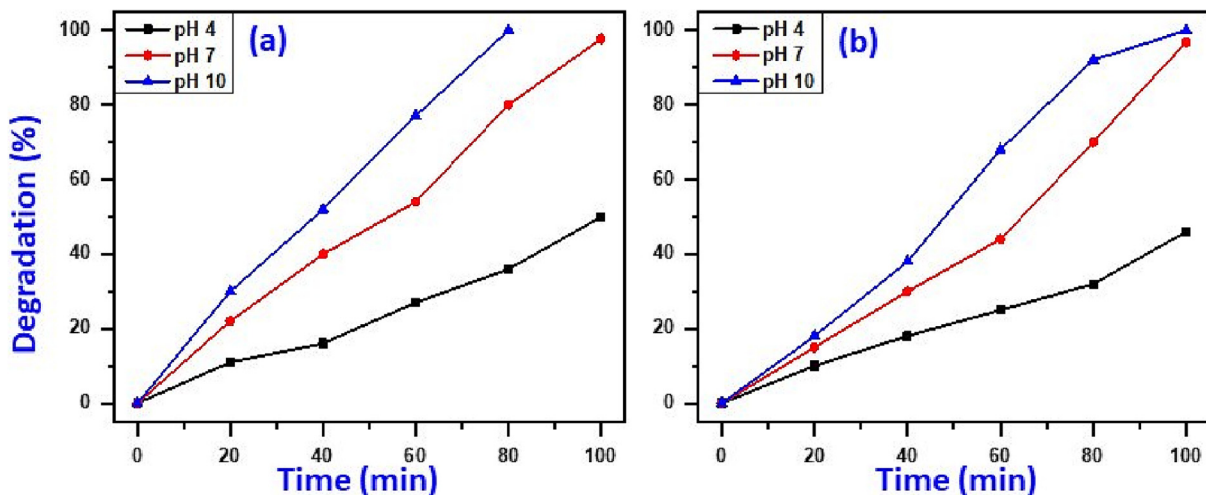


Fig. 7. Impact of pH on elimination of MB (a) and MG (b). (Circumstances: 15 mg catalyst dosage, 4 ppm dye conc., and UV-irradiation).

on the surface of catalyst. It is noteworthy to mention that the MB and MG are both positively charged cationic dyes that have a positive charge and the dyes can be easily adsorbed on the surface. Besides, higher quantities of hydroxyl radicals ( $\text{OH}^*$ ) were adsorbed on the catalyst surface and the photo-decomposition of dyes was conducted more efficaciously in alkaline medium (Farzana and Meenakshi 2014).

The kinetic results of photo-decomposition of MB and MG catalyzed by the prepared NiO-SD NPs obviously disclosed that the photo-catalytic elimination reaction takes places via Langmuir-Hinshelwood pseudo-1st-order reaction based on the subsequent formula (3)

$$\ln(C_i/C_f) = kt \tag{3}$$

The afore mentioned formula showed that  $C_i$  is initial concentration of dye at 0 min,  $C_f$  represents final concentration of dye at time  $t$  and the  $t$  (minutes) is the irradiation time, and  $k$  is rate constant. The MB photo-removal rate constants of 0.00656, 0.03316, and 0.18373  $\text{min}^{-1}$  were attained for pH 4, 7 and 10, respectively, as presented in Fig. 8a. However, the MG photo-

elimination rate constants of 0.00573, 0.02937, and 0.12605  $\text{min}^{-1}$  were calculated for pH 4, 7, and 10, respectively, as displayed in Fig. 8b.

Table 1 displays the comparison of photo-catalytic removal effectiveness of the present study with many already reported photocatalytic systems for removal of MB and MG. It is apparent that our photocatalyst in the current work possesses relatively superb photo-elimination efficiency for MB and MG.

### 3.7. Photo-degradation mechanism

Approach 2 demonstrates a probable scheme (Scheme S1) for the photo-elimination of MB and MG on surface of NiO-SD NPs. In presence of UV-irradiation, the electrons and holes were generated between valence-band (VB) and conduction-band (CB) of NiO-SD NPs. Hence, the photogenerated electrons ( $e^-$ ) formed in CB of NiO is scavenged by  $\text{O}_2$  to give anion radical ( $\text{O}_2^{\cdot-}$ ) and next reacted with proton ( $\text{H}^+$ ) produces  $^*\text{OOH}$ . However, the photogenerated holes ( $h^+$ ) were produced in VB of NiO will reacts with  $-\text{OH}$  or  $\text{H}_2\text{O}$  to produce extremely reactive species of hydroxyl radicals

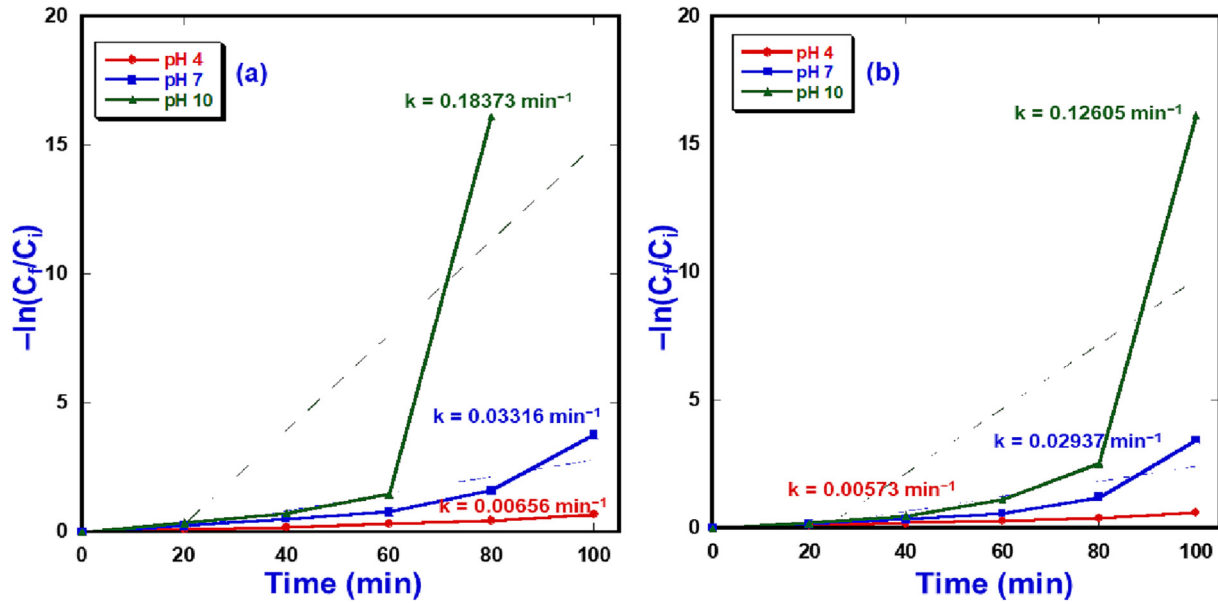


Fig. 8. Kinetics data of photo-breakdown of MB(a) and MG(b) over NiO-SD NPs photocatalyst.

Table 1

Photodecomposition performance comparison of the as-prepared NiO-SD NPs with other formerly reported photocatalysts for removal of MB and MG.

Photo-decomposition of MB						
Material	Time (min.)	Lighting source	Catalyst dosage	Conc. of dye	% of Degradation	Ref.
<b>NiO-SD NPs</b>	<b>100</b>	<b>UV-lamp</b>	<b>15 mg</b>	<b>4 ppm</b>	<b>100</b>	<b>Herein</b>
GO/TiO <sub>2</sub>	240	500 W Xe-lamp	0.2 g/L	5.0 ppm	99.0	(Kurniawan et al. 2020)
Ag-ZnO	30	Solar light	100 mg	10.0 ppm	98.5	(Stanley et al. 2021)
MnWO <sub>4</sub>	180	300 W W-lamp	50 mg	2.5 × 10 <sup>-5</sup> M	82.0	(Kumar et al. 2021)
Ag[Cu@Ag]	480	Solar light	2 g/L	10 ppm	40.7	(Miri and Ghorbani 2021)
ZnO-Au/Pd	180	200 W Xe-lamp	0.5 mg	5 × 10 <sup>-5</sup> M	97.0	(Lee et al. 2019)
chl/TiO <sub>2</sub>	120	14 W LED lamp	2.5 g/L	20 ppm	85.0	(Krishnan and Shrivastav 2021)
Mn <sub>3</sub> O <sub>4</sub> -rGO	120	Solar light	3 mg	1.0 ppm	60.0	(Jarvin, et al. 2021)
WO <sub>3</sub> -ZnO@rGO	90	200 W W-lamp	10 mg	5.0 ppm	94.0	(Chaudhary et al. 2020)
Ag <sub>3</sub> PO <sub>4</sub> /WO <sub>3</sub> ·H <sub>2</sub> O	30	300 W Xe-lamp	40 mg	10 ppm	98.9	(Tang et al. 2021)
Co/Ni-MOFs@BiOI	240	300 W PLSSXE	0.2 g/L	20 ppm	81.3	(Chen et al. 2021)
2%Fe-ZnO	180	150 WHg-lamp	10 mg	10 ppm	92.0	(Isai and Shrivastava 2019)
ZnO	120	10 W Hg-lamp	100 mg	15 ppm	90.0	(Soto-Robles et al. 2021)
Ag-ZnO@GO	180	20 W Xe-lamp	20 mg	15 ppm	85.0	(Tran Thi et al. 2019)
Photo-decomposition of MG						
<b>NiO-SD NPs</b>	<b>100</b>	<b>UV-lamp</b>	<b>15 mg</b>	<b>4 ppm</b>	<b>100</b>	<b>Herein</b>
GO/CuFe <sub>2</sub> O <sub>4</sub>	210	UV-lamp	0.01 g	5 × 10 <sup>-5</sup> M	90.7	(Yadav et al. 2021)
Gd-ZnS	10	160 W UV-bulb	100 mg	25 ppm	93.9	(Dhir 2021)
TiO <sub>2</sub> /Cellulose	60	UV-lamp	0.9 g/L	20 ppm	78.3	(Pang et al. 2021)
rGO-Fe <sub>3</sub> O <sub>4</sub> /TiO <sub>2</sub>	55	500 WHg-lamp	15 mg	5.5 ppm	99.0	(Bibi et al. 2021)
Fe-TiO <sub>2</sub> /AC	45	200 W UV-lamp	1.0 g/L	100 ppm	97.0	(Loo et al. 2021)
MnFe <sub>2</sub> O <sub>4</sub>	60	UV-lamp	30 mg	50 ppm	100	(de Andrade et al. 2021)
CuFe <sub>2</sub> O <sub>4</sub> @BC	90	UV-lamp	0.2 g/L	100 ppm	98.9	(Huang et al. 2021)
CoO Nanoparticles	100	Xe-lamp	0.5 g/L	1 × 10 <sup>-5</sup> M	91.2	(Verma et al. 2021)
La-ZnO/SiO <sub>2</sub>	140	300 W Xe-lamp	15 mg	15 ppm	96.1	(Wang et al. 2021)
CdSNanoparticles	60	300 W UV-lamp	50 mg	10 ppm	91.0	(Munyai et al. 2021)
BiVO <sub>4</sub> /g-C <sub>3</sub> N <sub>4</sub>	60	300 W Xe-lamp	1.0 g/L	30 ppm	98.3	(Li et al. 2021)
ZnO/CNT	60	200 W LED-lamp	10 mg	30 ppm	79.0	(Arsalani et al. 2020)
Co <sub>3</sub> O <sub>4</sub> /RP	20	300 W Xe-lamp	2 mg	20 ppm	94.5	(Tao et al. 2020)

\*OH. Consequently, the generated radical ions \*OH are in charge of the complete dye degradation, which leads to form lower harmful products like H<sub>2</sub>O and CO<sub>2</sub>. As a result, the photogenerated active species (\*OH and h<sup>+</sup>) are in charge of the breakdown of hazardous pollutants (MB and MG), and probable mechanism could be summarized as following equations.



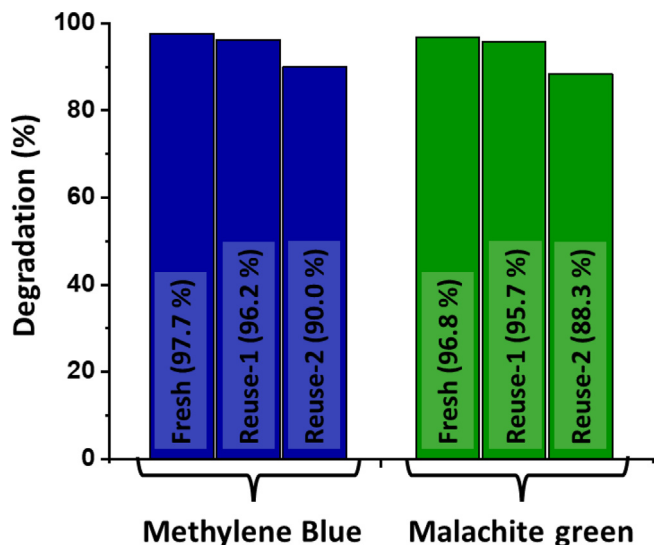


**Fig. 9.** Graphical illustration of reusability data of NiO-SD NPs against degradation of MB and MG dyes ([dye] = 4 ppm, dosage of NiO-SD NPs = 15 mg and pH 7).

According to the aforesaid equations, the photocatalytic decomposition of MB and MG was accomplished over NiO-SD NPs photocatalyst.

#### 4. Reusability of NiO-SD NPs

The utilized NiO-SD NPs are treated and used for the degradation of both MB and MG dyes under identical conditions as in detailed studies. The used photocatalyst was calcined at 300 °C and reused for the degradation of both MB and MG dyes at optimized condition of 15 mg catalyst, 4 ppm dye under pH 7 with the illumination of UV light. NiO-SD NPs showed performance as shown in the by Fig. 9. It can be observed that upon the first-time reuse there is a slight depreciation of catalytic activity, however upon reactivation of catalyst and reusing it for the second time, the results revealed that there is a significant depreciation in catalytic performance.

#### 5. Conclusions

In summing up, we have efficiently synthesized NiO-SD NPs, through an environmentally-benign, low cost, straightforward, and one-step combustion of sheep dung procedure. The characterization tools of the as-obtained catalyst confirmed that the cubic structure NiO-SD NPs phase. The fabricated NiO-SD NPs has been used for the photo catalytic decomposition of MB and MG as deleterious industrial pollutants. The results revealed that the NiO-SD NPs is effective and the removal effectiveness has been enormously affected by varying the lighting source, photocatalyst quantity, irradiation time, concentration of dye, and pH of medium. The as-synthesized photocatalyst NiO-SD NPs showed commendable photocatalytic efficacy (100%) of MB and MG dyes within 100 min at the optimum circumstances. It is noteworthy to note that the outstanding photo-elimination performance of NiO-SD NPs for removal of MB and MG, mainly attributed to electron-hole separation generated on NiO-SD NPs surface using UV-light. The low cost, environment-friendly, and highly efficient NiO-NPs with photocatalytic properties can be considered as an ideal material for wastewater treatment and related photo-catalytic applications.

#### Declaration of Competing Interest

The authors declare that they have no known competing financial interests or personal relationships that could have appeared to influence the work reported in this paper.

#### Acknowledgment

The authors acknowledge the funding from Researchers Supporting Project number (RSPD2023R665), King Saud University, Riyadh, Saudi Arabia.

#### Appendix A. Supplementary data

Supplementary data to this article can be found online at <https://doi.org/10.1016/j.jksus.2023.102784>.

#### References

- Alkbari, A., Sabouri, Z., Hosseini, H.A., Hashemzadeh, A., Khatami, M., Darroudi, M., 2020. Effect of nickel oxide nanoparticles as a photocatalyst in dyes degradation and evaluation of effective parameters in their removal from aqueous environments. *Inorganic Chemistry Communications* 115, 107867.
- Al Boukhari, J., Khalaf, A., Sayed Hassan, R., Awad, R., 2020. Structural, optical and magnetic properties of pure and rare earth-doped NiO nanoparticles. *Applied Physics A* 126 (5), 323.
- Alharthi, F.A., Al-Zaqri, N., El marghany, A., Alghamdi, A.A., Alorabi, A.Q., Baghdadi, N., Al-Shehri, H.S., Wahab, R., Ahmad, N., 2020. Synthesis of nanocauliflower ZnO photocatalyst by potato waste and its photocatalytic efficiency against dye. *Journal of Materials Science: Materials in Electronics* 31 (14), 11538–11547.
- Arsalani, N., Bazazi, S., Abuali, M., Jodeyri, S., 2020. A new method for preparing ZnO/CNT nanocomposites with enhanced photocatalytic degradation of malachite green under visible light. *Journal of Photochemistry and Photobiology A: Chemistry* 389, 112207.
- Asgharian, M., Mehdipourghazi, M., Khoshandam, B., Keramati, N., 2019. Photocatalytic degradation of methylene blue with synthesized rGO/ZnO/Cu. *Chemical Physics Letters* 719, 1–7.
- Barzinjy, A.A., Hamad, S.M., Aydin, S., Ahmed, M.H., Hussain, F.H.S., 2020. Green and eco-friendly synthesis of Nickel oxide nanoparticles and its photocatalytic activity for methyl orange degradation. *Journal of Materials Science: Materials in Electronics* 31 (14), 11303–11316.
- Belver, C., Bedia, J., Gómez-Avilés, A., Peñas-Garzón, M. and Rodríguez, J. J. 2019. Chapter 22 - Semiconductor Photocatalysis for Water Purification. *Nanoscale Materials in Water Purification*. S. Thomas, D. Pasquini, S.-Y. Leu and D. A. Gopakumar, Elsevier: 581–651.
- Bibi, S., Ahmad, A., Anjum, M.A.R., Haleem, A., Siddiq, M., Shah, S.S., Al Kahtani, A., 2021. Photocatalytic degradation of malachite green and methylene blue over reduced graphene oxide (rGO) based metal oxides (rGO-Fe<sub>3</sub>O<sub>4</sub>/TiO<sub>2</sub>) nanocomposite under UV-visible light irradiation. *Journal of Environmental Chemical Engineering* 9, (4) 105580.
- Capek, I. 2006. Chapter 1 Nanotechnology and nanomaterials. *Studies in Interface Science*. I. Capek, Elsevier: 23, 1–69.
- Chaudhary, K., Shaheen, N., Zulfiqar, S., Sarwar, M.I., Suleman, M., Agboola, P.O., Shakir, I., Warsi, M.F., 2020. Binary WO<sub>3</sub>-ZnO nanostructures supported rGO ternary nanocomposite for visible light driven photocatalytic degradation of methylene blue. *Synthetic Metals* 269, 116526.
- Chen, L., Ren, X., Alharbi, N.S., Chen, C., 2021. Fabrication of a novel Co/Ni-MOFs@BiOI composite with boosting photocatalytic degradation of methylene blue under visible light. *Journal of Environmental Chemical Engineering* 9, (5) 106194.
- Dalal, C., Garg, A.K., Jain, N., Naziruddin, A.R., Prajapati, R.K., Choudhary, S.K., Sonkar, S.K., 2023. Sunlight-assisted photocatalytic degradation of azo-dye using zinc-sulfide embedded reduced graphene oxide. *Solar Energy* 251, 315–324.
- de Andrade, F.V., de Oliveira, A.B., Siqueira, G.O., Lage, M.M., de Freitas, M.R., de Lima, G.M., Nuncira, J., 2021. MnFe<sub>2</sub>O<sub>4</sub> nanoparticulate obtained by microwave-assisted combustion: An efficient magnetic catalyst for degradation of malachite green cationic dye in aqueous medium. *Journal of Environmental Chemical Engineering* 9, (5) 106232.
- Dhir, R., 2021. Synthesis, characterization and applications of Gadolinium doped ZnS nanoparticles as photocatalysts for the degradation of dyes (Malachite Green and Rhodamine B) and as antioxidants. *Chemical Physics Impact* 3, 100027.
- Di, T., Xu, Q., Ho, W., Tang, H., Xiang, Q., Yu, J., 2019. Review on Metal Sulphide-based Z-scheme Photocatalysts. *ChemCatChem* 11 (5), 1394–1411.
- Farzana, M.H., Meenakshi, S., 2014. Synergistic effect of chitosan and titanium dioxide on the removal of toxic dyes by the photodegradation technique. *Industrial & Engineering Chemistry Research* 53 (1), 55–63.
- Fosso-Kankeu, E., Pandey, S., Ray, S.S., 2020. Photocatalysts in advanced oxidation processes for wastewater treatment. *John Wiley & Sons*.

- Gan, J.S., Li, X.B., Arif, U., Ali, F., Ali, A., Raziq, F., Ali, N., Yang, Y., Wang, Z., 2023. Development and characterization of silver modified novel graphitic-carbon nitride (Ag-ZnO/C<sub>3</sub>N<sub>4</sub>) coupled with metal oxide photocatalysts for accelerated degradation of dye-based emerging pollutants. *Surfaces and Interfaces* 102938.
- Gouadec, G., Colombar, P., 2007. Raman Spectroscopy of nanomaterials: How spectra relate to disorder, particle size and mechanical properties. *Progress in Crystal Growth and Characterization of Materials* 53 (1), 1–56.
- Hassan, M.A., El Nemr, A., Madkour, F.F., 2017. Testing the advanced oxidation processes on the degradation of Direct Blue 86 dye in wastewater. *Egyptian journal of aquatic research* 43 (1), 11–19.
- Huang, Q., Chen, C., Zhao, X., Bu, X., Liao, X., Fan, H., Gao, W., Hu, H., Zhang, Y., Huang, Z., 2021. Malachite green degradation by persulfate activation with CuFe<sub>2</sub>O<sub>4</sub>@ biochar composite: Efficiency, stability and mechanism. *Journal of Environmental Chemical Engineering* 9, (4) 105800.
- Isai, K.A., Shrivastava, V.S., 2019. Photocatalytic degradation of methylene blue using ZnO and 2% Fe-ZnO semiconductor nanomaterials synthesized by sol-gel method: a comparative study. *SN Applied Sciences* 1 (10), 1247.
- Jarvin, M., Kumar, S.A., Vinodhkumar, G., Manikandan, E., Inbanathan, S., 2021. Enhanced photocatalytic performance of Hausmannite Mn<sub>3</sub>O<sub>4</sub>-rGO nanocomposite in degrading methylene blue. *Materials Letters* 305, 130750.
- Jayakumar, G., Albert Irudayaraj, A., Dhayal Raj, A., 2017. Photocatalytic Degradation of Methylene Blue by Nickel Oxide Nanoparticles. *Materials Today: Proceedings* 4 (11, Part 3), 11690–11695.
- Khairnar, S.D., Shrivastava, V.S., 2019. Facile synthesis of nickel oxide nanoparticles for the degradation of Methylene blue and Rhodamine B dye: a comparative study. *Journal of Taibah University for Science* 13 (1), 1108–1118.
- Krishnan, S., Shrivastava, A., 2021. Application of TiO<sub>2</sub> nanoparticles sensitized with natural chlorophyll pigments as catalyst for visible light photocatalytic degradation of methylene blue. *Journal of Environmental Chemical Engineering* 9, (1) 104699.
- Kumar, M.S., Soundarya, T., Nagaraju, G., Raghu, G., Rekha, N., Alharthi, F.A., Nirmala, B., 2021b. Multifunctional applications of Nickel oxide (NiO) nanoparticles synthesized by facile green combustion method using Limonia acidissima natural fruit juice. *Inorganica Chimica Acta* 515, 120059.
- Kumar, K.S., Vaishnavi, K., Venkataswamy, P., Ravi, G., Ramaswamy, K., Vithal, M., 2021a. Photocatalytic degradation of methylene blue over N-doped MnWO<sub>4</sub> under visible light irradiation. *Journal of the Indian Chemical Society* 98, (10) 100140.
- Kurniawan, T.A., Mengting, Z., Fu, D., Yeap, S.K., Othman, M.H.D., Avtar, R., Ouyang, T., 2020. Functionalizing TiO<sub>2</sub> with graphene oxide for enhancing photocatalytic degradation of methylene blue (MB) in contaminated wastewater. *Journal of environmental management* 270, 110871.
- Lavand, A.B., Malghe, Y.S., 2015. Visible light photocatalytic degradation of 4-chlorophenol using C/ZnO/CdS nanocomposite. *Journal of Saudi Chemical Society* 19 (5), 471–478.
- Lee, S.J., Jung, H.J., Koutavarapu, R., Lee, S.H., Arumugam, M., Kim, J.H., Choi, M.Y., 2019. ZnO supported Au/Pd bimetallic nanocomposites for plasmon improved photocatalytic activity for methylene blue degradation under visible light irradiation. *Applied Surface Science* 496, 143665.
- Li, Y., Wang, X., Wang, X., Xia, Y., Zhang, A., Shi, J., Gao, L., Wei, H., Chen, W., 2021. Z-scheme BiVO<sub>4</sub>/g-C<sub>3</sub>N<sub>4</sub> heterojunction: an efficient, stable and heterogeneous catalyst with highly enhanced photocatalytic activity towards Malachite Green assisted by H<sub>2</sub>O<sub>2</sub> under visible light. *Colloids and Surfaces A: Physicochemical and Engineering Aspects* 618, 126445.
- Loo, W.W., Pang, Y.L., Lim, S., Wong, K.H., Lai, C.W., Abdullah, A.Z., 2021. Enhancement of photocatalytic degradation of Malachite Green using iron doped titanium dioxide loaded on oil palm empty fruit bunch-derived activated carbon. *Chemosphere* 272, 129588.
- Mahlaule-Glory, L.M., Mapetla, S., Makofane, A., Mathipa, M.M., Hintsho-Mbita, N.C., 2022. Biosynthesis of iron oxide nanoparticles for the degradation of methylene blue dye, sulfisoxazole antibiotic and removal of bacteria from real water. *Heliyon* 8 (9), e10536.
- Mills, A., Davies, R.H., Worsley, D., 1993. Water purification by semiconductor photocatalysis. *Chemical Society Reviews* 22 (6), 417–425.
- Mirgane, N.A., Shivankar, V.S., Kotwal, S.B., Wadhawa, G.C., Sonawale, M.C., 2021. Degradation of dyes using biologically synthesized zinc oxide nanoparticles. *Materials Today: Proceedings* 37, 849–853.
- Miri, A., Ghorbani, F., 2021. Syntheses of Ag [Cu@ Ag]@APTMS/boehmite as a photocatalyst for methylene blue degradation in batch and continuous flow systems under visible light. *Environmental Nanotechnology, Monitoring & Management* 16, 100493.
- Mironova-Ulmane, N., Kuzmin, A., Sildos, I., Puust, L., Grabis, J., 2019. Magnon and Phonon Excitations in Nanosized NiO. *Latvian Journal of Physics and Technical Sciences* 56 (2), 61–72.
- Munyai, S., Tetana, Z., Mathipa, M., Ntsendwana, B., Hintsho-Mbita, N., 2021. Green synthesis of Cadmium Sulphide nanoparticles for the photodegradation of Malachite green dye, Sulfisoxazole and removal of bacteria. *Optik* 247, 167851.
- Natarajan, S., Bajaj, H.C., Tayade, R.J., 2018a. Recent advances based on the synergetic effect of adsorption for removal of dyes from waste water using photocatalytic process. *Journal of Environmental Sciences* 65, 201–222.
- Natarajan, T.S., Thampai, K.R., Tayade, R.J., 2018b. Visible light driven redox-mediator-free dual semiconductor photocatalytic systems for pollutant degradation and the ambiguity in applying Z-scheme concept. *Applied Catalysis B: Environmental* 227, 296–311.
- Navarro, P., Gabaldón, J.A., Gómez-López, V.M., 2017. Degradation of an azo dye by a fast and innovative pulsed light/H<sub>2</sub>O<sub>2</sub> advanced oxidation process. *Dyes and Pigments* 136, 887–892.
- Nguyen, C.H., Fu, C.-C., Juang, R.-S., 2018. Degradation of methylene blue and methyl orange by palladium-doped TiO<sub>2</sub> photocatalysis for water reuse: Efficiency and degradation pathways. *Journal of Cleaner Production* 202, 413–427.
- Padre, S.M., Kiruthika, S., Mundinamani, S., Ravikiran, S., Surabhi, J.-R., Jeong, K.M., Eshwarappa, M.S., Murari, V., Shetty, M.B., C. G.S., 2022. Mono- and Bimetallic Nanoparticles for Catalytic Degradation of Hazardous Organic Dyes and Antibacterial Applications. *ACS Omega* 7 (39), 35023–35034.
- Pang, Y., Chuo, H., Lim, S., Chong, W., 2021. Photocatalytic degradation of malachite green using titanium dioxide immobilised on oil palm empty fruit bunch derived cellulose. *Materials Today: Proceedings* 46, 2017–2023.
- Patil, S.B., Ravishankar, T.N., Lingaraju, K., Raghu, G.K., Nagaraju, G., 2018. Multiple applications of combustion derived nickel oxide nanoparticles. *Journal of Materials Science: Materials in Electronics* 29 (1), 277–287.
- Pirhashemi, M., Habibi-Yangjeh, A., Pouran, S.R., 2018. Review on the criteria anticipated for the fabrication of highly efficient ZnO-based visible-light-driven photocatalysts. *Journal of industrial and engineering chemistry* 62, 1–25.
- Pouretedal, H.R., Norozi, A., Keshavarz, M.H., Semnani, A., 2009. Nanoparticles of zinc sulfide doped with manganese, nickel and copper as nanophotocatalyst in the degradation of organic dyes. *Journal of Hazardous Materials* 162 (2–3), 674–681.
- Qamar, Z., Khan, T.M., Abideen, Z.U., Shahzad, K., Hassan, A., Khan, S.U., Haider, S., Akhtar, M.S., 2022. Optical, morphological, and impedance characteristics of Ni (x)-(CdO)(1-x) nanofibers fabricated by electrospinning technique. *Materials Science and Engineering: B* 282, 115779.
- Ramesh, M., 2021. N and Fe doped NiO nanoparticles for enhanced photocatalytic degradation of azo dye methylene blue in the presence of visible light. *SN Applied Sciences* 3 (10), 817.
- Sabouri, Z., Akbari, A., Hosseini, H.A., Darroudi, M., 2018. Facile green synthesis of NiO nanoparticles and investigation of dye degradation and cytotoxicity effects. *Journal of Molecular Structure* 1173, 931–936.
- Salavati-Niasari, M., Mir, N., Davar, F., 2010. A novel precursor in preparation and characterization of nickel oxide nanoparticles via thermal decomposition approach. *Journal of Alloys and Compounds* 493 (1), 163–168.
- Singh, J., Dutta, T., Kim, K.-H., Rawat, M., Samddar, P., Kumar, P., 2018. 'Green' synthesis of metals and their oxide nanoparticles: applications for environmental remediation. *Journal of Nanobiotechnology* 16 (1), 84.
- Soto-Robles, C., Nava, O., Cornejo, L., Lugo-Medina, E., Vilchis-Nestor, A., Castro-Beltrán, A., Luque, P., 2021. Biosynthesis, characterization and photocatalytic activity of ZnO nanoparticles using extracts of *Justicia spicigera* for the degradation of methylene blue. *Journal of Molecular Structure* 1225, 129101.
- Stanley, R., Jebasingh, J.A., Stanley, P.K., Ponmani, P., Shekinah, M., Vasanthi, J., 2021. Excellent Photocatalytic degradation of Methylene Blue, Rhodamine B and Methyl Orange dyes by Ag-ZnO nanocomposite under natural sunlight irradiation. *Optik* 166518.
- Tammina, S.K., Mandal, B.K., Kadiyala, N.K., 2018. Photocatalytic degradation of methylene blue dye by nonconventional synthesized SnO<sub>2</sub> nanoparticles. *Environmental Nanotechnology, Monitoring & Management* 10, 339–350.
- Tang, J., Meng, R., Xue, Y., Zhang, S., Li, Q., 2021. Fabrication of a novel Ag<sub>3</sub>PO<sub>4</sub>/WO<sub>3</sub>-H<sub>2</sub>O composite with enhanced visible light photocatalytic performance for the degradation of methylene blue and oxytetracycline. *Inorganic Chemistry Communications* 132, 108792.
- Tao, J., Zhang, M., Gao, X., Zhao, H., Ren, Z., Li, D., Li, J., Zhang, R., Liu, Y., Zhai, Y., 2020. Photocatalyst Co<sub>3</sub>O<sub>4</sub>/red phosphorus for efficient degradation of malachite green under visible light irradiation. *Materials Chemistry and Physics* 240, 122185.
- Tran Thi, V.H., Pham, T.N., Pham, T.T., Le, M.C., 2019. Synergistic Adsorption and Photocatalytic Activity under Visible Irradiation Using Ag-ZnO/GO Nanoparticles Derived at Low Temperature. *Journal of Chemistry* 2019.
- Tsai, M.-J., Chung, M.-Y., Kuo, M.-Y., Wu, J.-Y., 2023. "Effective enhancement of performances on photo-assisted dye degradation using a Zn coordination polymer and its post-modified Cu/Zn bimetallic analogue under natural environments." *Journal of Environmental Chemical Engineering* 109258.
- Verma, M., Mitan, M., Kim, H., Vaya, D., 2021. Efficient photocatalytic degradation of Malachite green dye using facilely synthesized cobalt oxide nanomaterials using citric acid and oleic acid. *Journal of Physics and Chemistry of Solids* 155, 110125.
- Wang, S., Chen, Z., Zhao, Y., Sun, C., Li, J., 2021. High photocatalytic activity over starfish-like La-doped ZnO/SiO<sub>2</sub> photocatalyst for malachite green degradation under visible light. *Journal of Rare Earths* 39 (7), 772–780.
- Yadav, P., Suroli, P.K., Vaya, D., 2021. Synthesis and application of copper ferrite-graphene oxide nanocomposite photocatalyst for the degradation of malachite green. *Materials Today: Proceedings* 43, 2949–2953.
- Zhang, Z., Ma, Y., Bu, X., Wu, Q., Hang, Z., Dong, Z., Wu, X., 2018. Facile one-step synthesis of TiO<sub>2</sub>/Ag/SnO<sub>2</sub> ternary heterostructures with enhanced visible light photocatalytic activity. *Scientific reports* 8 (1), 1–11.
- Zollinger, H., 2003. *Color chemistry: syntheses, properties, and applications of organic dyes and pigments*. John Wiley & Sons.